MATERIALS SCIENCE

Chiral superconductivity in the alternate stacking compound 4Hb-TaS$_2$

A. Ribak[1]*, R. Majlin Skiff[2], M. Mograbi[2], P. K. Rout[2], M. H. Fischer[3], J. Ruhman[4], K. Chashka[1], Y. Dagan[2], A. Kanigel[1]†

Van der Waals materials offer unprecedented control of electronic properties via stacking of different types of two-dimensional materials. A fascinating frontier, largely unexplored, is the stacking of strongly correlated phases of matter. We study 4Hb-TaS$_2$, which naturally realizes an alternating stacking of 1T-TaS$_2$ and 1H-TaS$_2$ structures. The former is a well-known Mott insulator, which has recently been proposed to host a gapless spin-liquid ground state. The latter is a superconductor known to also host a competing charge density wave state. This raises the question of how these two components affect each other when stacked together. We find a superconductor with a T_c of 2.7 Kelvin and anomalous properties, of which the most notable one is a signature of time-reversal symmetry breaking, abruptly appearing at the superconducting transition. This observation is consistent with a chiral superconducting state.

INTRODUCTION

Chiral superconductors have received much attention in recent years as a canonical example of a topological phase of matter. Theoretically, they are predicted to host Majorana bound states in the vortex cores or at sample edges (1, 2), which have non-Abelian mutual statistics. Beyond the fundamental importance of observing such a phenomena, it has also been proposed as a useful technology for quantum memory and quantum computation (3). Chiral superconductors are characterized by an order parameter that is odd under time-reversal symmetry (TRS) and is manifested by magnetic fields at edges and defects (4). Therefore, they can be detected with probes such as muon spin relaxation (5) and polar Kerr effect (6).

Of all the known superconductors, only few exhibit signatures of TRS breaking, and even fewer are candidates for this elusive chiral phase. The best known among them are Sr$_2$RuO$_4$, believed to be of $p + ip$ symmetry (5), and UPt$_3$ (7), a potential $f + if$ superconductor, as well as the heavy-fermion superconductor URu$_2$Si$_2$ (8) and SrPtAs (9, 10), which were suggested to be of $d + id$ symmetry. Open questions remain, however, in all cases (11–13). Specifically, recent nuclear magnetic resonance measurements of Sr$_2$RuO$_4$ show a clear decrease in the Knight shift on entering the superconducting state, casting doubt on the p-wave nature of the superconducting order parameter (11).

In this work, we show evidence for chiral superconductivity in the transition-metal dichalcogenide 4Hb-TaS$_2$. We show that this polymorph of TaS$_2$ is a superconductor with a relatively high T_c and anomalous transport properties. 4Hb-TaS$_2$ exhibits a spontaneous appearance of magnetic moments with the onset of superconductivity.

4Hb-TaS$_2$ belongs to the P6$_3$/mmc hexagonal space group, with a unit cell that consists of alternating layers of 1H-TaS$_2$ (half of 2H-TaS$_2$) and 1T-TaS$_2$ (see Fig. 1A). The overall crystal is inversion symmetric, with the inversion point lying in the center of the 1T layer. The weak

interlayer coupling allows us to describe 4Hb-TaS$_2$ as a stack of two-dimensional (2D) monolayers: 1H-TaS$_2$ with a locally broken inversion symmetry giving rise to antisymmetric spin-orbit coupling (14) and 1T-TaS$_2$, known as a Mott insulator that fails to order magnetically (15). Recently, it was proposed that the ground state of 1T-TaS$_2$ is a gapless quantum spin liquid (16, 17, 18). Thus, 4Hb-TaS$_2$ is a system in which superconducting layers naturally reside in proximity to layers that have strong spin fluctuations. Consequently, it realizes a unique heterostructure of strongly correlated phases with drastically different ground states, albeit having the exact same chemical composition and almost the same structure.

RESULTS

We have grown single crystals of 4Hb-TaS$_{2-x}$Se$_x$ with $x = 0.01$, using a standard chemical vapor transport method (19). The small amount of Se stabilizes the 4Hb structure. Details about the sample preparation process and the structure characterization appear in the Supplementary Materials.

4Hb-TaS$_2$ was first synthesized by Di Salvo et al. (19). The transport data can be described as a mixture of 1T and 2H, with metallic conductivity in the ab plane and semiconducting conductivity along the c axis. The in-plane resistivity was shown to be three orders of magnitude smaller than the out-of-plane resistivity. This "mixture" of 1T and 2H is also visible in the x-ray photoelectron spectroscopy spectrum of the Ta $4f$ core levels, which displays three peaks—two from the "1T" layers and one from the "1H" layers (fig. S2) (20).

The electronic dispersion along the Γ-M direction was measured using angle-resolved photoemission spectroscopy (ARPES) and is presented in Fig. 1D. The main finding is that the band structure of the 4Hb-TaS$_2$ is a mixture of the metallic 2H layer and the band structure of the 1T shifted toward the Fermi level, leaving no spectral gap. This should be compared with the 1T structure where a band-gap of 0.2 eV was measured and interpreted as a Mott gap (21, 22). The parts of the band structure associated with the 1T and the 1H layers are marked in the figure.

Two electron pockets, similar to the ones in 2H-TaS$_2$, can be observed surrounding the points $k = \pm 1/\text{Å}$ together with the shifted band structure of 1T-TaS$_2$. The 1T part of the band structure is

[1]Physics Department, Technion-Israel Institute of Technology, Haifa 32000, Israel.
[2]Raymond and Beverly Sackler School of Physics and Astronomy, Tel-Aviv University, Tel Aviv 69978, Israel. [3]Department of Physics, University of Zurich, 8057 Zurich, Switzerland. [4]Department of Physics, Bar-Ilan University, Ramat Gan 5290002, Israel.
*Present address: Max Planck Institute for the Structure and Dynamics of Matter, Hamburg 22761, Germany.
†Corresponding author. Email: amitk@physics.technion.ac.il
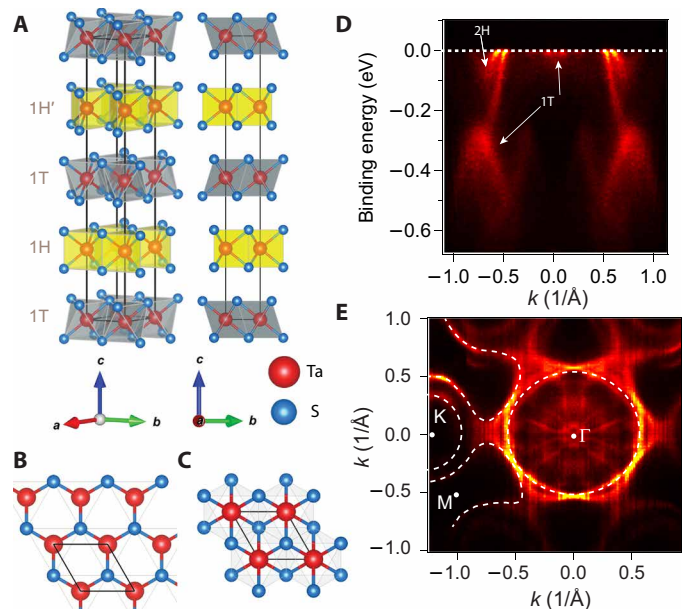
Fig. 1. Structure of 4Hb-TaS₂. (**A**) 3D schematic drawing of a unit cell of 4Hb-TaS₂ showing the alternate stacking of octahedral (T) and trigonal prismatic (H) layers. Top views of 1H and 1T layers are shown in (**B**) and (**C**), respectively. The top view of the 1H layer displays the in-plane broken mirror symmetry. (**D**) An ARPES detector image obtained at T = 15 K using 72 eV of photon energy reveals the electronic band structure along the Γ-M direction. (**E**) A Fermi surface mapping under the same conditions. The band structure is a combination of 2H-TaS₂ and CDW reconstructed 1T-TaS₂, which was rigidly shifted toward the Fermi level [horizontal white dashed line in (D)]. The dashed line represents the 2H-TaS₂ Fermi surface.

reconstructed by the well-known $\sqrt{13} \times \sqrt{13}$ charge density wave (CDW).

An ARPES intensity map at the Fermi level is shown in Fig. 1E. The intensity map reveals that within the alternate-stacking layered crystal, every layer retains its original electronic dispersion. The Fermi surface is a mixture of the Fermi surface of 2H-TaS₂ with its familiar dog-bone–shaped pockets around the M points and the reconstructed 1T-TaS₂ bands contribution around the Γ point.

Figure 2A shows C_e/T versus T, where C_e is the electronic part of the specific heat after the removal of the phonon contribution (for details, see the Supplementary Materials). The transition into a superconducting state below $T_c \approx 2.7$ K is seen both in specific heat and resistance measurements (see inset in Fig. 2B), which is substantially enhanced compared to bulk 2H-TaS₂ (T_c = 0.7 K). The enhancement is most likely the result of the 1T layers that create a buffer layer between the 1H and 1H′ layers. A similar enhancement was observed in 2H-TaS₂ samples, where a buffer layer was intercalated (*23*, *24*), and in 2D flakes (*25*, *26*).

The heat capacity $C_e(T)$ also exhibits a residual linear-in-T contribution observed below T_c (finite intersect in the $T \to 0$ limit marked by the dotted line in Fig. 2A). This residual contribution is independent of magnetic field and amounts to 15% of the normal-state heat capacity (dashed line). Furthermore, it has been reproduced in samples from different growth batches showing the same magnitude, supporting that this residual contribution is an intrinsic effect relevant to the physics in 4Hb-TaS₂.

After the subtraction of the residual heat capacity, we obtain a standard s-wave–like shape that decays exponentially to zero (Fig. 2B). The extracted gap Δ is found to be 0.4 ± 0.05 meV(see the Supple-
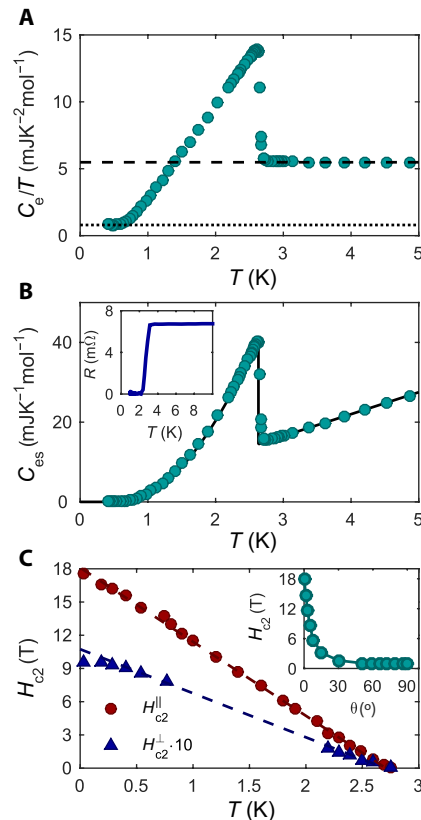
Fig. 2. Specific heat and transport measurements. (**A**) The electronic contribution to the heat capacity divided by the temperature C_e/T is plotted as function of T. The dashed line represents the total electronic specific heat in the normal state, and the dotted line is a residual linear contribution coming from the 1T layers (see the main text for details). (**B**) The electronic-specific heat after the removal of the 1T contribution displaying a BCS-type behavior with Δ = 0.4 meV. Inset: Resistance versus temperature shows enhanced T_c. (**C**) H_{c2} as a function of temperature for in-plane (red circles) and out-of-plane (blue triangles) field orientations. For better visibility, $H_{c2}^{\perp}$ is multiplied by 10. Inset: The angular dependence of H_{c2} showing strong anisotropy.

mentary Materials for more details), in good agreement with the transverse field muon spin rotation (μSR) results shown in the Supplementary Materials. Thus far, the picture emerging is that of a fully gapped superconductor coexisting with a second phase with a constant density of states, at least down to an energy resolution equivalent to 300 mK.

In the inset of Fig. 2C, we show the critical field, H_{c2}, as a function of the angle θ, between the applied field and the *ab* plane (θ = 0 denotes field aligned in the plane), measured at T = 30 mK. The magneto-resistance exhibits strong anisotropy, with $H_{c2}^{\parallel}/H_{c2}^{\perp} > 17$. The angular dependence of H_{c2}, plotted in the inset, is consistent with the predictions of a highly anisotropic Ginzburg-Landau theory (see the Supplementary Materials), reflecting the quasi-2D nature of superconductivity in 4Hb-TaS₂.

We also note that a naïve calculation of the Clogston-Chandrasekhar limit using the estimated minimal gap from the exponential decay of the specific heat (see the Supplementary Materials) $\Delta_0^{\min}$ = 0.36 meV, yields a paramagnetic limit of H_p = 5 T, much smaller than the observed $H_{c2}^{\parallel}$. Moreover, because of strong Ising spin-orbit coupling, we anticipate the critical Zeeman field to greatly exceed this value (*27*).

The quasi-2D picture is further supported by the temperature dependence of $H_{c2}^{\parallel}$ shown in Fig. 2C. We observe an unusual linear dependence of the in-plane critical field through the entire temperature range. Similar behavior has been reported in Bi_2Se_3 under pressure (28), where it was interpreted as a result of a polar p-wave state, and also in KOs_2O_6, where it was ascribed to a multiband effect (29). We note that the Zeeman-limited H_{c2} typically results in a nonlinear temperature dependence, and thus, we argue that even the in-plane field is most likely orbitally limited.

To extract coherence lengths from the orbital limited fields, we use the highly anisotropic Ginzburg-Landau theory. The in-plane coherence length is found from the perpendicular critical field (see Fig. 2C) $\xi_{ab} = \sqrt{\frac{\phi_0}{2\pi H_c^{\perp}}} = 186$ Å, and using $H_{c2}^{\parallel} = \frac{\phi_0}{\xi_{ab}\xi_c}$, we find the out-of-plane coherence length to be $\xi_c = 9.8$ Å. This length is comparable to the interlayer spacing of 1H layers. We can therefore conclude that $4Hb$-TaS_2 is a stack of weakly coupled 2D superconductors with weak orbital out-of-plane tunneling currents.

We now turn to the main result of our work: evidence of TRS breaking in the superconducting state seen in a μSR measurement. In the absence of a magnetic order, the muon depolarization is a result of the randomly oriented static nuclear dipole moments and is described by the static Gaussian Kubo-Toyabe function (30)

$$G_z(t) = \frac{1}{3} + \frac{2}{3}\left(1 - \sigma^2 t^2\right)\exp\left(-\frac{1}{2}\sigma^2 t^2\right) \qquad (1)$$

where σ/γ_μ is the local field distribution width, and γ_μ is the muon gyromagnetic ratio. The nuclear field distribution is temperature independent.

In Fig. 3, we show the temperature dependence of the muon depolarization rate in the absence of a magnetic field. We find an abrupt increase of the rate at $T = T_c$. This is a clear indication of a spontaneous appearance of magnetic moments in the sample due to the superconducting state. In the inset of Fig. 3, we present two representative Zero Field muon spin resonance spectra, above and below T_c (at 6 and 0.05 K, respectively). On the basis of the increase in σ, we estimate the width of the randomly oriented magnetic field in the sample to be ~0.12 G.
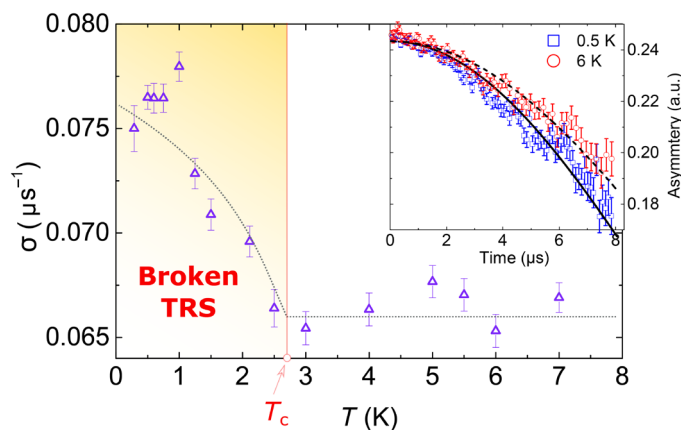
Fig. 3. TRS breaking. A sudden increase in the zero-field muon spin relaxation rate σ is observed at T_c (marked by the vertical line), marking the onset of TRS breaking. The dotted line is a guide to the eye. The inset shows two ZF-μSR spectra at different temperatures, above and below T_c. The black lines are best fits to Eq. 1.

Theoretical interpretation

With the onset of TRS breaking coinciding with the superconducting T_c, it is natural to assume an origin intrinsic to the superconducting phase for this TRS breaking. This leads to chiral superconductivity as a compelling explanation of TRS breaking: In such a state, magnetic moments are expected to appear due to local variations in the chiral order parameter resulting, for example, from edges or defects in the sample (4). Such a state is allowed by the hexagonal point group symmetry of $4Hb$-TaS_2 as we discuss below. While there are other scenarios that can account for signatures of TRS breaking within a superconducting phase, notably, combinations of nearly degenerate symmetry-distinct order parameters or frustrated interband Cooper-pair scattering, these generically happen not at T_c but at a distinctly lower temperature (9). Thus, the most probable picture emerging from the data is that of a quasi-2D fully gapped chiral superconductor.

In the following, we discuss topological properties of such a chiral state. The weak interlayer coupling discussed above motivates us to study the superconducting state on isolated 1H layers with point group symmetry D_{3h}. With TRS present in the normal state, chiral superconductivity requires a multicomponent gap function. Within the relevant symmetry group, there is only one such representation (31), which allows us to pinpoint the gap function

$$\Delta_E(\boldsymbol{k}) = \Delta_0\left[(1-\alpha)e_{\boldsymbol{k}}\sigma^0 + \alpha o_{\boldsymbol{k}}^*\sigma^z\right]i\sigma^y \qquad (2)$$

where $e_{\boldsymbol{k}} = \sum_{j=1}^{3}\omega^j\cos(\boldsymbol{k}\cdot\boldsymbol{T}_j)$ and $o_{\boldsymbol{k}} = \sum_{j=1}^{3}\omega^j\sin(\boldsymbol{k}\cdot\boldsymbol{T}_j)$ are the d-wave and p-wave basis functions in the D_{3h} point group. Here, we have chosen only one chirality, in other words, only Cooper pairs with positive orbital angular momentum, while their negative counterparts are given by complex conjugation. The vectors $\pm\boldsymbol{T}_j$ point to the six nearest neighbors on the triangular Ta lattice, $\omega = \exp(2\pi i/3)$, and α is a non-universal weight, which quantifies the mixing of the d-wave and p-wave components that is allowed by the lack of an inversion center in the plane. Last, σ^0 and σ^i denote the identity and Pauli matrices. Note that because of the alternate stacking of the 1H layers, the relative phase of the order parameters in Eq. 2 changes from layer to layer (31).

Chiral superconductivity belongs to symmetry class D in the 10-fold way (32), which allows us to classify isolated 1H layers using a Chern number. Using a tight-binding model for TaS_2 including up to the third-nearest-neighbor hopping (27, 33), we compute the Chern number within a BdG Hamiltonian as a function of α, allowing us to interpolate between the pure $d + id$- and $p + ip$-wave pairing channels. The phase of the superconducting order parameter in Eq. 2 is presented in Fig. 4 (A and B) for the extreme cases α = 0 (purely d-wave) and α = 1 (purely p-wave), respectively. We find that the Chern number vanishes in the limit of α = 0, i.e., $C = 0$, because the inner and outer Fermi surfaces cancel each other. On the other hand, the Chern density is cooperative in the limit α = 1, where we obtain $C = -6$. The interpolation between these two points is plotted in Fig. 4C. Note that the data points were computed numerically (not rounded to an integer) using the full BdG band structure with a mesh grid of 9.5×10^4 equally spaced points. Overall, we find that the Chern number of the Chiral state is highly sensitive to the mixing ratio α (34). A challenging experimental goal is thus to measure a quantized thermal Hall conductance in this system.
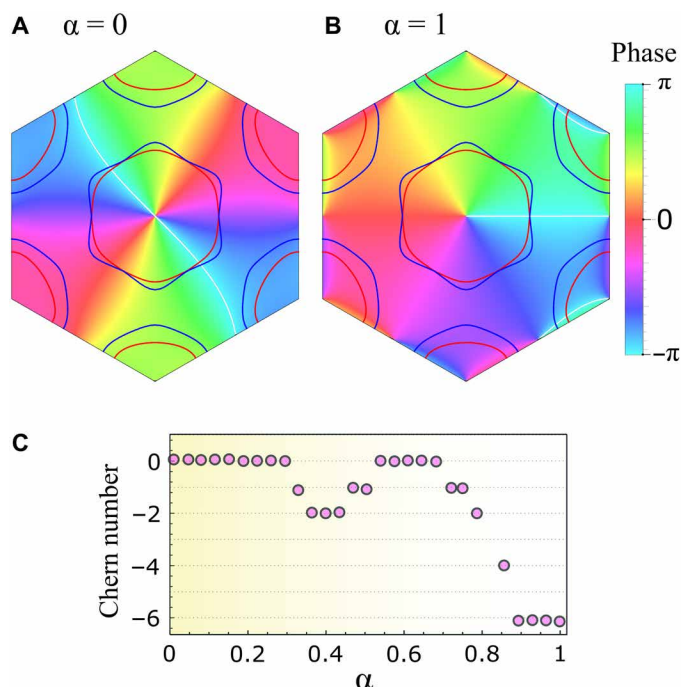
Fig. 4. Superconducting order parameter. (**A**) and (**B**) show the phase of the gap functions $e_\mathbf{k}$ and $o_\mathbf{k}$, respectively, superimposed on the Fermi surface of 1H-TaS$_2$. (**C**) The corresponding Chern number as a function of the mixing parameter α appearing in Eq. 2. Note that the values presented here were computed numerically and are not rounded to an integer.

DISCUSSION

We first address the question of the residual linear heat capacity observed below T_c (Fig. 2A). The scenario of macroscopic phase separation, where portions of the sample remain metallic, can be ruled out by the Transverse field muon spin rotation data. The TF-μSR measurements were performed in field cooling conditions, and we found 100% superconducting volume fraction at base temperature. Furthermore, we found only small sample-to-sample variation in the magnitude of this residual term.

A possible scenario is that the proximity gap induced in 1T layers is much smaller than the gap in the 1H and 1H′ layers, thus a temperature lower than our base temperature of 300 mK will be needed to suppress the contribution of the 1T layers to the specific heat. This is a plausible explanation given the large Fermi surface mismatch shown in Fig. 1E, which naturally leads to a weak proximity effect.

Another possible explanation for the linear heat capacity is a spin-glass state (35), forming at the 1T layers. The x-ray analysis indicates highly clean crystal structure and, therefore, any mechanism leading to such a state must be intrinsic (e.g., frustrated interactions). However, this state seems unlikely given that the time dependence of the μSR signal does not fit the classic glass behavior (36, 37). Moreover, the magnitude of the residual is independent of field, and lastly, no spin-glass behavior in the susceptibility has been observed in earlier studies (23).

A more exotic scenario is that this contribution is coming from a neutral Fermi surface coexisting with the superconducting state. A gapless spin-liquid state has been proposed for the 1T polytype of TaS$_2$ (16, 17).

We now turn to the microscopic origin of the possible chiral superconductivity. Phonon-mediated interactions typically favor s-wave pairing (38). In such a case, unconventional pairing is expected only if strong local repulsion, which reduces the attraction in the s-wave channel, is present. On the other hand, an attractive interaction mediated by spin fluctuations naturally prefers non–s-wave superconductivity and, in particular, chiral symmetry when the Fermi surface encloses the Γ point as given here (see Fig. 1E). From this perspective, it is interesting to understand whether the proximity between the superconductor in the 1H layers and the Mott insulating state in the 1T layers is an essential ingredient. Our ARPES data in Fig. 1E suggest the possibility that the Mott insulator is lightly doped due to the stacking structure, resulting in strong spin fluctuations. Electronic pairing mediated by spin fluctuations in a quantum spin ice has been studied in (39) for the case of a rotationally symmetric Fermi surface. There, the authors found that the strongest pairing channel is odd-parity with the possibility of a multicomponent order parameter, consistent with the chiral superconductor proposed here. The results presented here, thus, raise a host of theoretical questions regarding the interaction between superconductivity, charged, and neutral itinerant fermionic excitations, which invite further study.

To summarize, we have investigated 4Hb-TaS$_2$ and found signs of TRS breaking in the form of an abrupt rise in the muon relaxation rate upon cooling below the superconducting transition temperature. Given the hexagonal symmetry and the Fermi surface topology, these findings suggest that 4Hb-TaS$_2$ is a chiral superconductor. We further show that the unique structure of 4Hb-TaS$_2$ consisting of stacked, weakly coupled layers of 1H-TaS$_2$ and 1T-TaS$_2$ results in a band structure, which combines the properties of both constituents: a 2D superconductor (1H) and a doped Mott insulator proposed to be a gapless spin liquid (1T). Both constituents show clear signatures both in ARPES and in the low-temperature specific heat. Its relatively high superconducting $T_c \simeq 2.7$ K, the quasi-2D structure, and the ability to grow very large and clean single crystals make this material a promising platform for future study and applications. Furthermore, it opens new directions in the study of topological superconductivity using van der Waals heterostructures.

MATERIALS AND METHODS

High-quality single crystals of 4Hb-TaS$_2$ were prepared using the chemical vapor transport method. The appropriate amounts of Ta and S were ground and mixed with a small amount of Se (1% of the S amount). The powder was sealed in a Quartz ampoule, and a small amount of iodine was added as a transport agent. The ampoule was placed in a three-zone furnace such that the powder is in the hot zone. After 30 days, single crystals with a typical size of 5 mm × 5 mm × 0.1 mm grew in the cold zone of the furnace.

High-resolution ARPES measurements were performed at the I05 beamline at Diamond (Didcot, UK) and at the SIS Beamline at the SLS (Villigen, Switzerland) using a photon energy of 72 eV. The samples were cleaved in vacuum better than 5×10^{-11} torr at base temperature and measured for not more than 6 hours. The samples were measured at a temperature of 10 K. The energy resolution was 6 meV in both beamlines.

Both zero-field and transverse-field μSR measurements were performed at the DOLLY beamline at PSI (Villigen, Switzerland) over a temperature range from 7 K down to 300 mK. The transverse-field measurements were performed using a 145-G field.

Heat capacity measurements at various fields were performed using Quantum Design PPMS He3 probe. The addenda was measured in all fields and temperatures to ensure proper background subtraction.

Transport properties were measured using standard lock-in technique in a dilution refrigerator equipped with an 18-T magnet and a rotator probe at the Tallahassee National Laboratory. For the higher temperature range, a He3 probe in a PPMS was used.

SUPPLEMENTARY MATERIALS

Supplementary material for this article is available at http://advances.sciencemag.org/cgi/content/full/6/13/eaax9480/DC1

Section S1. Crystal growth and characterization
Section S2. Electrical transport and magnetization measurements
Section S3. Heat capacity measurements
Section S4. Muon spin rotation measurements
Section S5. Gap structure
Fig. S1. X-ray diffraction of 4Hb-TaS$_2$ single crystals.
Fig. S2. XPS spectrum of 4Hb-TaS$_2$.
Fig. S3. Transport measurements.
Fig. S4. Heat capacity measurements.
Fig. S5. Muon spin relaxation results.
Fig. S6. Tight-binding band structure.
References (40–47)

REFERENCES AND NOTES

1. N. Read, D. Green, Paired states of fermions in two dimensions with breaking of parity and time-reversal symmetries and the fractional quantum Hall effect. *Phys. Rev. B.* **61**, 10267–10297 (2000).
2. J. D. Sau, R. M. Lutchyn, S. Tewari, S. Das Sarma, Generic new platform for topological quantum computation using semiconductor heterostructures. *Phys. Rev. Lett.* **104**, 40502 (2010).
3. C. Nayak, S. H. Simon, A. Stern, M. Freedman, S. Das Sarma, Non-Abelian anyons and topological quantum computation. *Rev. Mod. Phys.* **80**, 1083–1159 (2008).
4. M. Sigrist, K. Ueda, Phenomenological theory of unconventional superconductivity. *Rev. Mod. Phys.* **63**, 239–311 (1991).
5. G. M. Luke, Y. Fudamoto, K. M. Kojima, M. I. Larkin, J. Merrin, B. Nachumi, Y. J. Uemura, Y. Maeno, Z. Q. Mao, Y. Mori, H. Nakamura, M. Sigrist, Time-reversal symmetry-breaking superconductivity in Sr$_2$RuO$_4$. *Nature* **394**, 558 (1998).
6. J. Xia, Y. Maeno, P. T. Beyersdorf, M. M. Fejer, A. Kapitulnik, High resolution polar kerr effect measurements of Sr$_2$RuO$_4$: Evidence for broken time-reversal symmetry in the superconducting state. *Phys. Rev. Lett.* **97**, 167002 (2006).
7. E. R. Schemm, W. J. Gannon, C. M. Wishne, W. P. Halperin, A. Kapitulnik, Observation of broken time-reversal symmetry in the heavy-fermion superconductor UPt$_3$. *Science* **345**, 190–193 (2014).
8. I. Kawasaki, I. Watanabe, A. Hillier, D. Aoki, Time-reversal symmetry in the hidden order and superconducting states of URu$_2$Si$_2$. *J. Phys. Soc. Jpn.* **83**, 094720 (2014).
9. P. K. Biswas, H. Luetkens, T. Neupert, T. Stürzer, C. Baines, G. Pascua, A. P. Schnyder, M. H. Fischer, J. Goryo, M. R. Lees, H. Maeter, F. Brückner, H.-H. Klauss, M. Nicklas, P. J. Baker, A. D. Hillier, M. Sigrist, A. Amato, D. Johrendt, Evidence for superconductivity with broken time-reversal symmetry in locally noncentrosymmetric SrPtAs. *Phys. Rev. B* **87**, 180503 (2013).
10. M. H. Fischer, T. Neupert, C. Platt, A. P. Schnyder, W. Hanke, J. Goryo, R. Thomale, M. Sigrist, Chiral d-wave superconductivity in SrPtAs. *Phys. Rev. B* **89**, 020509 (2014).
11. A. Pustogow, Y. Luo, A. Chronister, Y.-S. Su, D. A. Sokolov, F. Jerzembeck, A. P. Mackenzie, C. W. Hicks, N. Kikugawa, S. Raghu, E. D. Bauer, S. E. Brown, Constraints on the superconducting order parameter in Sr$_2$RuO$_4$ from oxygen-17 nuclear magnetic resonance. *Nature* **574**, 72–75 (2019).
12. E. Hassinger, P. Bourgeois-Hope, H. Taniguchi, S. René de Cotret, G. Grissonnanche, M. S. Anwar, Y. Maeno, N. Doiron-Leyraud, L. Taillefer, Vertical line nodes in the superconducting gap structure of Sr$_2$RuO$_4$. *Phys. Rev. X* **7**, 011032 (2017).
13. E. R. Schemm, E. M. Levenson-Falk, A. Kapitulnik, Polar Kerr effect studies of time reversal symmetry breaking states in heavy fermion superconductors. *Phys. C Supercond. Appl.* **535**, 13–19 (2017).
14. M. H. Fischer, F. Loder, M. Sigrist, Superconductivity and local noncentrosymmetricity in crystal lattices. *Phys. Rev. B* **84**, 184533 (2011).
15. P. Fazekas, E. Tosatti, Charge carrier localization in pure and doped 1T-TaS$_2$. *Phys. B+C* **99**, 183–187 (1980).
16. K. T. Law, P. A. Lee, 1T-TaS$_2$ as a quantum spin liquid. *Proc. Natl. Acad. Sci. U.S.A.* **114**, 6996–7000 (2017).
17. A. Ribak, I. Silber, C. Baines, K. Chashka, Z. Salman, Y. Dagan, A. Kanigel, Gapless excitations in the ground state of 1T–TaS$_2$. *Phys. Rev. B* **96**, 195131 (2017).
18. H. Murayama, Y. Sato, X. Z. Xing, T. Taniguchi, S. Kasahara, Y. Kasahara, M. Yoshida, Y. Iwasa, Y. Matsuda, Coexisting localized and itinerant gapless excitations in a quantum spin liquid candidate 1T-TaS$_2$. arXiv:1803.06100 (2018).
19. F. J. Di Salvo, B. G. Bagley, J. M. Voorhoeve, J. V. Waszczak, Preparation and properties of a new polytype of tantalum disulfide 4Hb-TaS$_2$. *J. Phys. Chem. Solid* **34**, 1357–1362 (1973).
20. H. P. Hughes, J. A. Scarfe, Site specific photohole screening in a charge density wave. *Phys. Rev. Lett.* **74**, 3069–3072 (1995).
21. L. Perfetti, T. A. Gloor, F. Mila, H. Berger, M. Grioni, Unexpected periodicity in the quasi-two-dimensional Mott insulator 1T–TaS$_2$ revealed by angle-resolved photoemission. *Phys. Rev. B* **71**, 153101 (2005).
22. R. Ang, Y. Tanaka, E. Ieki, K. Nakayama, T. Sato, L. J. Li, W. J. Lu, Y. P. Sun, T. Takahashi, Real-space coexistence of the melted mott state and superconductivity in Fe-Substituted 1T–TaS$_2$. *Phys. Rev. Lett.* **109**, 176403 (2012).
23. J. A. Wilson, F. J. Di Salvo, S. Mahajan, Charge-density waves and superlattices in the metallic layered transition metal dichalcogenides. *Adv. Phys.* **24**, 117–201 (1975).
24. A. H. Thompson, F. R. Gamble, R. F. Koehler Jr., Effects of intercalation on electron transport in tantalum disulfide. *Phys. Rev. B* **5**, 2811–2816 (1972).
25. E. Navarro-Moratalla, J. O. Island, S. Mañas-Valero, E. Pinilla-Cienfuegos, A. Castellanos-Gomez, J. Quereda, G. Rubio-Bollinger, L. Chirolli, J. A. Silva-Guillén, N. Agraït, G. A. Steele, F. Guinea, H. S. J. van der Zant, E. Coronado, Enhanced superconductivity in atomically thin TaS$_2$. *Nat. Commun.* **7**, 11043 (2016).
26. Y. Yang, S. Fang, V. Fatemi, J. Ruhman, E. Navarro-Moratalla, K. Watanabe, T. Taniguchi, E. Kaxiras, P. Jarillo-Herrero, Enhanced superconductivity upon weakening of charge density wave transport in 2H-TaS$_2$ in the two-dimensional limit. *Phys. Rev. B* **98**, 035203 (2018).
27. D. Möckli, M. Khodas, Robust parity-mixed superconductivity in disordered monolayer transition metal dichalcogenides. *Phys. Rev. B* **98**, 144518 (2018).
28. K. Kirshenbaum, P. S. Syers, A. P. Hope, N. P. Butch, J. R. Jeffries, S. T. Weir, J. J. Hamlin, M. B. Maple, Y. K. Vohra, J. Paglione, Pressure-induced unconventional superconducting phase in the topological insulator Bi$_2$Se$_3$. *Phys. Rev. Lett.* **111**, 087001 (2013).
29. T. Shibauchi, L. Krusin-Elbaum, Y. Kasahara, Y. Shimono, Y. Matsuda, R. D. McDonald, C. H. Mielke, S. Yonezawa, Z. Hiroi, M. Arai, T. Kita, G. Blatter, M. Sigrist, Uncommonly high upper critical field of the pyrochlore superconductor KOs$_2$O$_6$ below the enhanced paramagnetic limit. *Phys. Rev. B* **74**, 220506 (2006).
30. R. S. Hayano, Y. J. Uemura, J. Imazato, N. Nishida, T. Yamazaki, R. Kubo, Zero-and low-field spin relaxation studied by positive muons. *Phys. Rev. B* **20**, 850–859 (1979).
31. J. Goryo, M. H. Fischer, M. Sigrist, Possible pairing symmetries in SrPtAs with a local lack of inversion center. *Phys. Rev. B* **86**, 100507 (2012).
32. S. Ryu, A. P. Schnyder, A. Furusaki, A. W. W. Ludwig, Topological insulators and superconductors: Tenfold way and dimensional hierarchy. *New J. Phys.* **12**, 65010 (2010).
33. G.-B. Liu, W.-Y. Shan, Y. Yao, W. Yao, D. Xiao, Three-band tight-binding model for monolayers of group-VIB transition metal dichalcogenides. *Phys. Rev. B* **88**, 085433 (2013).
34. B. Zinkl, M. H. Fischer, M. Sigrist, Superconducting gap anisotropy and topological singularities due to lattice translational symmetry and their thermodynamic signatures. *Phys. Rev. B* **100**, 014519 (2019).
35. K. Binder, A. P. Young, Spin glasses: Experimental facts, theoretical concepts, and open questions. *Rev. Mod. Phys.* **58**, 801–976 (1986).
36. M. I. Larkin, Y. Fudamoto, I. M. Gat, A. Kinkhabwala, K. M. Kojima, G. M. Luke, J. Merrin, B. Nachumi, Y. J. Uemura, M. Azuma, T. Saito, M. Takano, Crossover from dilute to majority spin freezing in two leg ladder system Sr(Cu,Zn)$_2$O$_3$. *Phys. Rev. Lett.* **85**, 1982–1985 (2000).
37. A. Kanigel, A. Keren, Y. Eckstein, A. Knizhnik, J. S. Lord, A. Amato, Common energy scale for magnetism and superconductivity in underdoped cuprates: A muon spin resonance investigation of (Ca$_x$La$_{1-x}$)(Ba$_{1.75-x}$La$_{0.25+x}$)Cu$_3$O$_y$. *Phys. Rev. Lett.* **88**, 137003 (2002).
38. P. M. R. Brydon, S. Das Sarma, H.-Y. Hui, J. D. Sau, Odd-parity superconductivity from phonon-mediated pairing: Application to Cu$_x$Bi$_2$Se$_3$. *Phys. Rev. B* **90**, 184512 (2014).
39. J.-H. She, C. H. Kim, C. J. Fennie, M. J. Lawler, E.-A. Kim, Topological superconductivity in metal/quantum-spin-ice heterostructures. *npj Quantum Mater.* **2**, 64 (2017).
40. Y. Liu, L. J. Li, W. J. Lu, R. Ang, X. Z. Liu, Y. P. Sun, Coexistence of superconductivity and commensurate charge density wave in 4H$_b$-TaS$_{2-x}$Se$_x$ single crystals. *J. Appl. Phys.* **115**, 043915 (2014).
41. G. K. Wertheim, F. J. DiSalvo, S. Chiang, Charge-density waves and many-body effects in x-ray photoelectron spectroscopy of layer-structure chalcogenides. *Phys. Rev. B* **13**, 5476–5483 (1976).

42. H. P. Hughes, R. A. Pollak, Charge density waves in layered metals observed by X-ray photoemission. *Philos. Mag. A J. Theor. Exp. Appl. Phys.* **34**, 1025–1046 (1976).

43. K. Ishizaka, T. Kiss, T. Yamamoto, Y. Ishida, T. Saitoh, M. Matsunami, R. Eguchi, T. Ohtsuki, A. Kosuge, T. Kanai, M. Nohara, H. Takagi, S. Watanabe, S. Shin, Femtosecond core-level photoemission spectroscopy on 1T-TaS$_2$ using a 60-eV laser source. *Phys. Rev. B* **83**, 081104 (2011).

44. J. A. Scarfe, H. P. Hughes, Core-level lineshapes in photoemission from transition-metal intercalates of TaS$_2$. *J. Phys. Condens. Matter* **1**, 6865 (1989).

45. H. Padamsee, J. E. Neighbor, C. A. Shiffman, Quasiparticle phenomenology for thermodynamics of strong-coupling superconductors. *J. Low Temp. Phys.* **12**, 387–411 (1973).

46. D. C. Johnston, Elaboration of the α-model derived from the BCS theory of superconductivity. *Supercond. Sci. Technol.* **26**, 115011 (2013).

47. M. Tinkham, *Introduction to Superconductivity* (Dover Publications Inc., Mineola, N.Y, Ed. 2, 2004).

Citation: A. Ribak, R. M. Skiff, M. Mograbi, P. K. Rout, M. H. Fischer, J. Ruhman, K. Chashka, Y. Dagan, A. Kanigel, Chiral superconductivity in the alternate stacking compound 4Hb-TaS$_2$. *Sci. Adv.* **6**, eaax9480 (2020).

Chiral superconductivity in the alternate stacking compound 4Hb-TaS$_2$

A. Ribak, R. Majlin Skiff, M. Mograbi, P. K. Rout, M. H. Fischer, J. Ruhman, K. Chashka, Y. Dagan and A. Kanigel